Control of Lipid Domain Organization by a Biomimetic Contractile Actomyosin Cortex

Sven K. Vogel[1†], Ferdinand Greiss[1,2,3†], Alena Khmelinskaia[1,3] and Petra Schwille[1]

[1]Max-Planck Institute of Biochemistry, Am Klopferspitz 18, D-82152 Martinsried, Germany
[2]Systems Biophysics, Physics Department, Ludwig-Maximilans-University, Amalienstr. 54, D-80799 Munich, Germany
[3]Graduate School of Quantitative Biosciences, Ludwig-Maximilans-University, Feodor-Lynen-Str. 25, D-81377 Munich, Germany

[†] Contributed equally

Abstract

The cell membrane is a heterogeneously organized composite with lipid-protein micro-domains. The contractile actin cortex may govern the lateral organization of these domains in the cell membrane, yet the underlying mechanisms are not known. We recently reconstituted minimal actin cortices (MACs) (Vogel et al, 2013b) and here advanced our assay to investigate effects of rearranging actin filaments on the lateral membrane organization by introducing various phase-separated lipid mono- and bilayers to the MACs. The addition of actin filaments reorganized membrane domains. We found that the process reached a steady state where line tension and lateral crowding balanced. Moreover, the phase boundary allowed myosin driven actin filament rearrangements to actively move individual lipid domains, often accompanied by their shape change, fusion or splitting. Our findings illustrate how actin cortex remodeling in cells may control dynamic rearrangements of lipids and other molecules inside domains without directly binding to actin filaments.

Introduction

The spatiotemporal organization of lipids, proteins and other molecules at and within the cell membrane is pivotal for many fundamental cellular processes, such as signal transduction from the extracellular to the intracellular space (Groves & Kuriyan, 2010). Recent findings suggest that the cell membrane should be considered as a heterogeneous lipid protein layer with coexisting small micro domains and clusters of lipids and proteins that are assumed to dynamically form and reorganize in response to external and internal cues (Engelman, 2005; Simons & Gerl, 2010). Whether and how their spatiotemporal organization is actively regulated and maintained by the cell remains to be revealed. *In vivo* and *in vitro* studies suggest an important role of the eukaryotic actin cytoskeleton that interacts with the cell membrane via membrane-associated proteins (Heinemann et al, 2013; Koster et al, 2016; Murase et al, 2004; Sheetz et al, 1980). Actin structures were found to mediate the lateral organization of membrane proteins (Gudheti et al, 2013) and to modulate their diffusive behavior (Heinemann et al, 2013; Honigmann et al, 2014; Murase et al, 2004). Theoretical considerations have proposed a key role of the actin motor myosin for organizing and forming distinct protein and lipid micro-domains in cell membranes (Gowrishankar et al, 2012). However, direct experimental evidence for a control of lipid micro-domains by actomyosin rearrangements is still lacking.

In eukaryotic cells, the actin cortex is constantly rearranged by the motor protein myosin II and dozens of actin binding proteins. Therefore, reducing the complexity of experimental conditions, e.g. reducing dimensionality or exploiting a minimal biomimetic system, and utilizing microscopic techniques with a high temporal resolution is beneficial for studying these processes. Phase-separated lipid bilayers with controlled lipid compositions are well-established test beds to mimic lipid micro-domains in cell membranes and biological processes, e.g. the lateral organization of proteins that are otherwise difficult to observe *in vivo*. Ternary mixtures of lipids below their characteristic melting temperature (Tm) can phase separate into liquid disordered (L_d) and liquid ordered (L_o) domains. Liu and Fletcher used phase-separated giant unilamellar vesicles (GUVs) as a model system to study the influence of branched actin networks on the miscibility transition temperature (Liu & Fletcher, 2006). They reported that the formation of localized actin networks on PIP_2-containing phase-separated GUVs could act as switch for the orientation of lipid

domain growth sites.

However, the effects of an actin meshwork on individual lipid domains are technically difficult to study, due to the 3-dimensional architecture of the GUVs. We therefore made use of a minimal biomimetic system of planar geometry that we recently developed (Vogel et al, 2013a; Vogel et al, 2013b) and combined the minimal actin cortex (MAC) with supported phase-separated membranes and free-standing lipid monolayers. We then visualized and studied the effects of actin filament adhesion and myosin driven rearrangements on the lateral organization of membrane domains with total internal reflection microscopy (TIRFM) and confocal spinning disk microscopy.

Results

Actin filament partitioning on phase-separated membranes

The effects of adhesion and myosin induced contraction of an actin meshwork on the lateral organization of lipid domains was studied by combining phase-separated lipid membranes with our established assay featuring contractile MACs (Vogel, 2016; Vogel et al, 2013a; Vogel et al, 2013b) (Fig. 1A). For the adhesion assay a ternary lipid mixture with DOPC, DPPC and Cholesterol in a 1:2:1 molar ratio was prepared (see Material and Methods). Similar lipid compositions were described to form L_o and L_d phases in free-standing membranes up to 30 °C (Veatch & Keller, 2003; Veatch & Keller, 2005). The low miscibility transition temperature of the mixture avoids thermal degradation of proteins and allowed us to study the phase transition behavior in the presence of actin filaments. The fluorescent probe DiD (0.03 mol%) was used to label the L_d phases (Garcia-Saez et al, 2007). The density of biotinylated actin filaments was controlled by the concentration of biotinylated lipid DSPE-PEG(2000)-Biotin (see also (Vogel, 2016; Vogel et al, 2013b)). As observed with TIRF microscopy, the membrane separated into micrometer-sized L_o and L_d domains (Fig. 1B-E) and homogenized at ~37 ºC. The observed shift of 7 °C in Tm compared with studies from (Veatch & Keller, 2003) agreed with our expectations considering the interaction of lipid molecules with the mica support (Garcia-Saez et al, 2007).

The adhesion of actin filaments via neutravidin to biotinylated DSPE provided a stable link between the MAC and the lipid bilayer over a wide range of temperatures.

104 To validate the partitioning preference of all molecular components, the fluorescence
105 signals of labeled neutravidin and actin filaments were acquired after domain
106 formation when cooled below Tm (Fig. 1B-E). We found that both neutravidin and
107 actin filaments partitioned into the L_o phase (Fig. 1B and C). We therefore concluded
108 that the biotinylated lipid DSPE partitioned strongly to the L_o phase.
109
110 **Actin filament crowding effects on supported phase-separated membranes**
111 We prepared low (0.01 mol % DSPE-PEG(2000)-Biotin) and medium (0.1 mol %
112 DSPE-PEG(2000)-Biotin, Fig. 2B) dense MACs to investigate the effect of actin
113 filament density on phase-separated membranes. To this end, the ternary lipid mixture
114 was incubated with non-labeled neutravidin and placed on a temperature-controlled
115 microscope objective. A fluorescence image was acquired as a reference before actin
116 filaments were added (Fig. 2A and B (left column)). A homogeneous membrane was
117 produced by heating the microscope objective to 42 °C (above Tm). Actin filaments
118 were added to the membrane above Tm (Fig. 2A and B (middle column)) and the
119 sample was subsequently incubated for ~45 min at 42 °C (Fig. 2A). The membrane
120 was completely covered by actin filaments after approximately 30 minutes (Fig. 2A
121 and B (middle column)). As final step, the membrane was slowly cooled down to 30
122 °C without active cooling and the fluorescence signal was recorded after complete
123 phase separation (Fig. 2A and B (right column)). While the low density MAC did not
124 show any influence on membrane domain properties (data not shown), the medium
125 dense MAC caused the formation of smaller domains (Fig. 2B, right column). Both,
126 actin filaments and DSPE-PEG(2000)-Biotin partitioned into the L_o phase (Fig. 2B
127 and C), confirming our initial observations (Fig. 1B - E). We conclude that actin
128 filaments act as nucleation sites for domain formation and drive their lateral spatial
129 distribution reproducing the observations reported by Honigmann et al (Honigmann et
130 al, 2014).
131 To further investigate the relation between lateral membrane organization and the
132 binding of actin filaments, we exposed high density MACs containing a lipid mixture
133 with 1.0 mol% biotinylated DSPE to different temperatures below Tm (Fig. 2C - F).
134 Fluorescently labeled actin filaments were added to the sample chamber at specified
135 temperatures below Tm and imaged for ~30 min using TIRF microscopy (Fig. 2C).
136 Because of the strong binding affinity of neutravidin and biotin, we found that the
137 change in fluorescence intensity of labeled actin filaments (which we used as a

138 measure for actin filament binding) was independent of the applied temperature (Fig.
139 2F). Hence, the adhesion process of actin filaments to the membrane was constant
140 over the employed temperature range. The contour length (L) (Fig. 2G) of membrane
141 domains was extracted and tracked over time (Fig. 2D). After ~1 min of actin filament
142 addition, first domain deformations could be observed and the contour length was
143 found to grow until a steady state at ~20 min was reached (Fig. 2D). The final contour
144 length increased with temperature (Fig. 2E, final change in contour length: L_{Final}
145 = 188±4 µm and τ = 9.5±0.5 min at 24 °C, L_{Final} = 314.0±1.5 µm and τ = 5.6±0.1 min
146 at 29 °C, L_{Final} = 706.3±2.5 µm and τ = 4.4±0.1 min at 32 °C). The line tension γ
147 between L_o and L_d domains is known to be a linear function of temperature with
148 $\gamma \approx \gamma_0(T_C - T)/T_C$ where T_C is the critical temperature (Baumgart et al, 2003;
149 Honerkamp-Smith et al, 2008; Veatch et al, 2008). With the temperature-independent
150 actin filament binding and the boundary energy given by $E = \gamma L$ (Yang et al, 2016)
151 where E is the boundary energy, the final contour length L should increase with
152
153 $$L = \frac{E}{\gamma_0}\frac{T_C}{T_C - T}\,. \qquad (1)$$
154
155 The model describes the experimental data well (Fig. 2E) and gives a length change
156 (E/γ_0) of 86±9 µm at T = 0 °C with T_C = 37 °C.
157
158 **Actomyosin contraction governs lateral membrane domain organization**
159 Aster shaped actomyosin clusters form *in vivo* (Luo et al, 2013; Munro et al, 2004;
160 Verkhovsky et al, 1997) and *in vitro* (Backouche et al, 2006; Koster et al, 2016;
161 Murrell & Gardel, 2012; Soares e Silva et al, 2011; Vogel et al, 2013b) upon myosin's
162 contractile activity. Synthetic myofilaments contract the MAC in the presence of ATP
163 and, hence rearrange actin filaments to form stable actomyosin clusters (Fig. 3A, C
164 and G; Video 1 and 5). For studying the effects of myofilament induced actin
165 rearrangements we prepared two lipid mixtures for lipid mono- and bilayer
166 experiments, namely DOPC, DPPC and Cholesterol in a 1:2:1 molar ratio and DOPC,
167 PSM and Cholesterol in a 3:3:1 molar ratio containing 0.1 or 1 mol% DSPE-
168 PEG(2000)-Biotin DSPE (see Material and Methods).
169 We found that upon contraction, membrane domains deformed at the phase
170 boundaries within minutes and resulted in various splitting and fusion events (Fig. 3A,

171 D, F and G; Videos 2-4 and 6). Domain shape changes, such as inward ingression,
172 were observed and correlated with the movement of actomyosin clusters (Fig. 3D;
173 Videos 3 and 4). Actomyosin contraction against smaller L_d domains resulted in their
174 net movement and occasionally led to splitting events of the domain (Fig. 3D; Video
175 4) while the contraction for L_o domains led to deformation and fusion with
176 neighboring domains (Fig. 3F; Video 6). For both mixtures the area of the L_o phase
177 remained constant over the course of actomyosin contraction (Fig. 3B and E, left
178 panels). The number of L_d domains increased with time due to their splitting for the
179 DOPC, DPPC, Cholesterol mixture (Fig. 3B, right panel; Videos 2-4). The number of
180 L_o domains decreased in the DOPC, PSM, Cholesterol mixture due to their fusion and
181 occasional disappearance during actomyosin contraction (Fig. 3E (right panel) and G;
182 Videos 6 and 7). A similar behavior in L_o domain disappearance has been observed by
183 Koster et al (Koster et al, 2016). In contrast to their work we did not observe a
184 decrease of the total L_o phase domain area in neither of the lipid mixtures (Fig. 3B
185 and E, left panels). In summary, we showed active lateral reorganization of lipid
186 domains for two different lipid mixtures, indicating the general validity of our
187 experimental observations.
188
189 In order to mimic free-standing membranes without support-induced friction as in the
190 SLBs but keeping the technical advantages of a planar geometry, we made use of a
191 recently developed lipid monolayer system (Chwastek & Schwille, 2013) with an air-
192 liquid interface (Fig. 4A - D). Actin filaments were coupled to ternary phase-
193 separated lipid monolayers similar to the situation in the supported lipid bilayer (SLB)
194 system via biotinylated lipids (1 mol%) and the use of neutravidin. Contrary to the
195 situation in the SLB system, actin filaments preferentially bind to the liquid extended
196 (disordered) (L_e) phase where also the neutravidin anchor protein mainly partitioned
197 to (Fig. 4A - D). We observed this behavior for both lipid mixtures that were also
198 used for the SLBs (see Material and Methods). In low and medium dense monolayer
199 MACs the liquid condensed (ordered) L_c domains acquire circular shapes and the
200 actin filaments close to the phase boundaries align to their circular shape (Fig. 4A). In
201 the case of low and medium densities we expect that the line tension energy
202 dominates over the actin filament wetting energy at the phase boundary and hence the
203 L_c can assume an unrestricted shape with aligned actin filaments. Similar effects have
204 been observed using bacterial cytoskeleton proteins (Arumugam et al, 2015). The

205 addition of myosin filaments in the presence of ATP led to the contraction of the actin
206 layer deforming and rearranging the L_c domains in both lipid mixtures similar to what
207 we observed in the SLB systems (Fig. 4B – D; Video 8). The shape changes included
208 fusion and stretching of the L_c domains (Fig. 4B – D; Video 8). Note that these
209 "active" deformation forces were only exerted in the presence of myosin filaments
210 and ATP. Interestingly, the obtained lipid domain shapes seemed to be stabilized after
211 the active contraction period, probably by the remaining actin filaments. Using the
212 monolayer system also tells us that the frictional force caused by a solid support in
213 SLBs does not play a significant role in the observed phenomena.
214

215 **Discussion**

216 As cells may need to quickly adapt the macro-and microscopic organization of lipid
217 and protein aggregates within the cell membrane due to external or internal cues, we
218 propose that actomyosin driven reorganization of actin filaments may aid to quickly
219 govern their lateral distribution. Recent evidence exists that the presence of an actin
220 meshwork influences the lateral diffusion behavior of lipids and proteins in
221 membranes *in vivo* (Murase et al, 2004) and *in vitro* (Heinemann et al, 2013) and that
222 it impacts the behavior of phase-separated membranes (Honigmann et al, 2014; Liu &
223 Fletcher, 2006). The important role of myosin is further supported by recent
224 theoretical and *in vitro* studies (Gowrishankar et al, 2012; Koster et al, 2016). It is
225 therefore tempting to speculate that cortical actomyosin contractility may be a generic
226 model for eukaryotic organisms not only to control their mechanical stability and
227 shape but also to quickly and actively control the lateral lipid and protein organization
228 at the cell membrane.
229 In our MACs that were combined with ternary lipid mixtures we found that binding of
230 actin filaments to a homogeneous bilayer at temperatures above Tm induced spatial
231 alignment of L_o domains to actin bound locations upon cooling below Tm (Fig. 2).
232 Here, actin filaments serve as nucleation sites for domain formation and drive their
233 lateral spatial distribution. Already phase separated, we could show that membrane
234 domains reorganized with the adhesion of actin filaments depending on line tension
235 and actin filament density. We further give direct evidence that the dynamic
236 reorganization of actin filaments by myosin motors actively changes the macroscopic
237 organization of membrane domains in our reconstituted phase-separated lipid bilayers

238 and monolayers. We propose that the transition energy between the L_d and L_o phase
239 (Baumgart et al, 2003; Garcia-Saez et al, 2007; Honerkamp-Smith et al, 2008)
240 enabled the lipid anchored actin filaments to exert lateral forces on the phase
241 boundaries leading to a macroscopic motion of lipid domains that eventually resulted
242 in splitting, fusion or deformation of the lipid domains and in their overall change in
243 number during and after the actomyosin contraction (Fig. 3 B and E, right panels;
244 Videos 2-4, 6 and 8). In a model we would first consider a biotinylated lipid that is
245 dragged by an actomyosin filament (Fig. 4E). The actomyosin filaments are unequally
246 associated with the lipid phases (L_o and L_d) with different viscosities. The drag is
247 counteracted by friction and, through the different viscosities, leads to domain
248 deformation and rearrangement. Here, the force propagation would be independent of
249 phase boundaries. As a second consideration, the biotinylated lipid would need to
250 overcome the transition barrier between phases while being dragged over a boundary
251 (Fig. 4E). Since our contraction experiments primarily showed that the boundaries
252 deformed locally at actin filament sites and that actomyosin foci formed at the vicinity
253 of phase boundaries, the high transition energy is favored as the dictating driving
254 force for phase deformation. Furthermore, domain deformation was commonly found
255 to happen when actin filaments were dragged over the L_d phase that impedes the free
256 contraction process through the strong partitioning preference of DSPE-PEG(2000)-
257 Biotin to the L_o phase.
258 With an estimated line tension of 1 pN for a 1:2:1 DOPC:DPPC:Cholesterol
259 membrane (Baumgart et al, 2003; Garcia-Saez et al, 2007; Kuzmin et al, 2005; Veatch
260 & Keller, 2005) and a reported value of ~1.5 k_BT for the transfer of DPPC between
261 phases (Veatch et al, 2004), the energy for one DPPC molecule to transition is
262 roughly 6-fold higher than the energy that is needed to elongate the phase boundary
263 by 1 nm. Further experiments should elaborate on the physical model since
264 actomyosin contraction is clearly a non-equilibrium process and line tension itself was
265 reported to depend on the applied lateral tension (Akimov et al, 2007). Together with
266 our experimental findings, we can conclude that actively rearranging actin filaments
267 will lead to an extensive deformation of membrane domains through the physical link
268 with a small subset of membrane constituents. A plausible mechanism is therefore
269 apparent that explains active lateral rearrangements of membrane components by
270 actomyosin contractions without the need of binding directly to actin filaments.

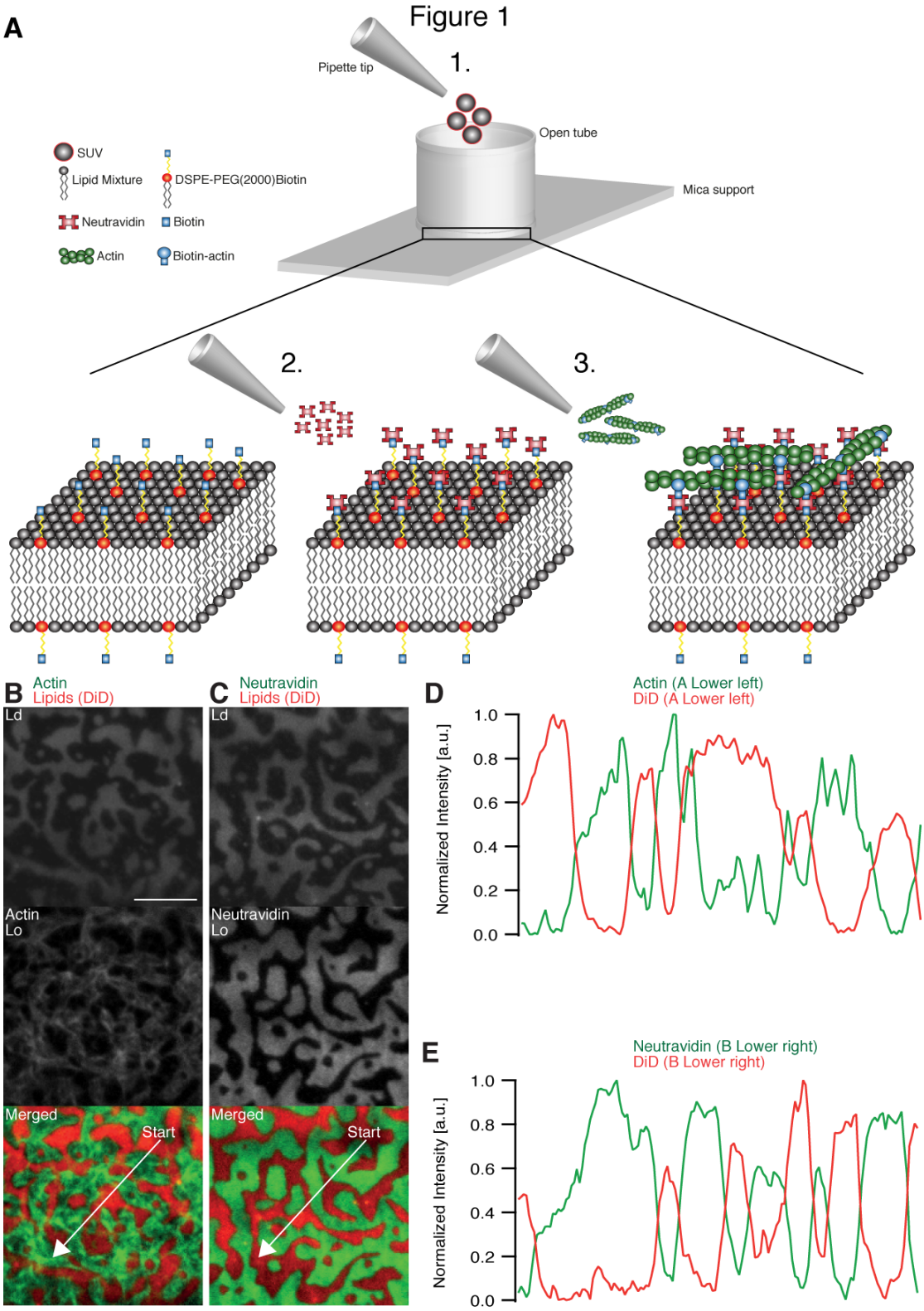

Fig. 1. Minimal actin cortex on supported phase-separated lipid membranes. (A) Illustration depicting the preparation of the SLB and the coupling of actin filaments to the membrane (Adapted from (Vogel et al, 2013a)). (B) Since DiD is known to partition specifically to the L_d phase (1:2:1 DOPC:DPPC:Cholesterol), the fluorescence signal of Alexa-488-phalloidin labeled actin filaments showed that DSPE-PEG(2000)-Biotin partitioned into the L_o phase. (C) Likewise, Oregon Green labeled neutravidin colocalized with the L_o phase. (D and E) Line profiles of the normalized fluorescence signal of the actin cortex, DiD and neutravidin as was measured along the superimposed arrows in (B) and (C). Scale bar, 10 μm.

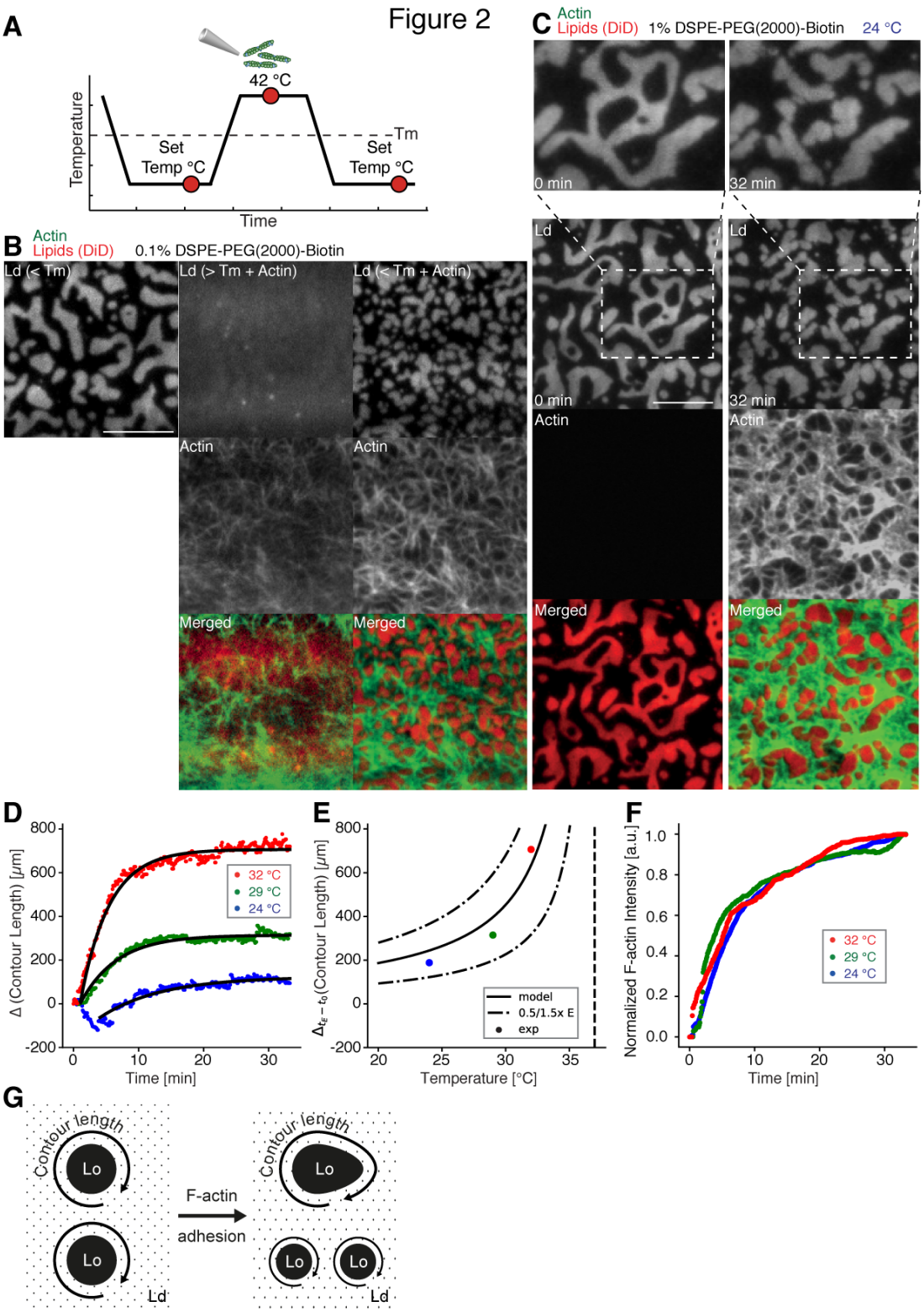

Fig. 2. Impact of actin filaments on the lateral organization of phase-separated membranes. (A) Scheme of a phase separation experiment with and without MAC is shown with circles indicating time points when fluorescent images were acquired. (B) Size distribution of lipid domains changed in the presence of a MAC while undergoing phase separation. TIRF images of a medium dense MAC with DiD labeled L_d phase (1:2:1 DOPC:DPPC:Cholesterol) are shown below Tm (30 °C) (left column), above Tm (42 °C) in the presence of bound Alexa-488-phalloidin labeled actin filaments (middle column) and below Tm (30 °C) in the presence of bound actin (right column). The final size of L_d domains decreased through the presence of actin filaments. (C) Change in contour length through the binding of actin

filaments to the already phase-separated membrane at various temperatures below Tm. A high density MAC with a DiD labeled L_d phase before (0 min) and after the addition (32 min) of actin filaments at 24 ºC is shown. (D) Contour length of L_d domains upon F-actin adhesion with time and mono-exponential decay fits at 24 ºC (blue dots), 29 ºC (green dots) and 32 ºC (red dots). (Note that the observed local dip in contour length between 2 and 5 min at 24 ºC is because of a focal misalignment and blurring of the images after the addition of actin filaments). (E) Final change in contour length for the different temperatures. With a constant lateral pressure, the linearly decreasing line tension with temperature leads to an increase in final contour length according to equation (1). Dashed vertical line indicates Tm of 37 ºC. (F) The binding kinetics of actin filaments was tracked with the normalized fluorescence signal over time at 24 ºC (blue dots), 29 ºC (green dots) and 32 ºC (red dots). (G) Illustrative sketch for the change in contour length before and after F-actin adhesion. Scale bars, 10 μm.

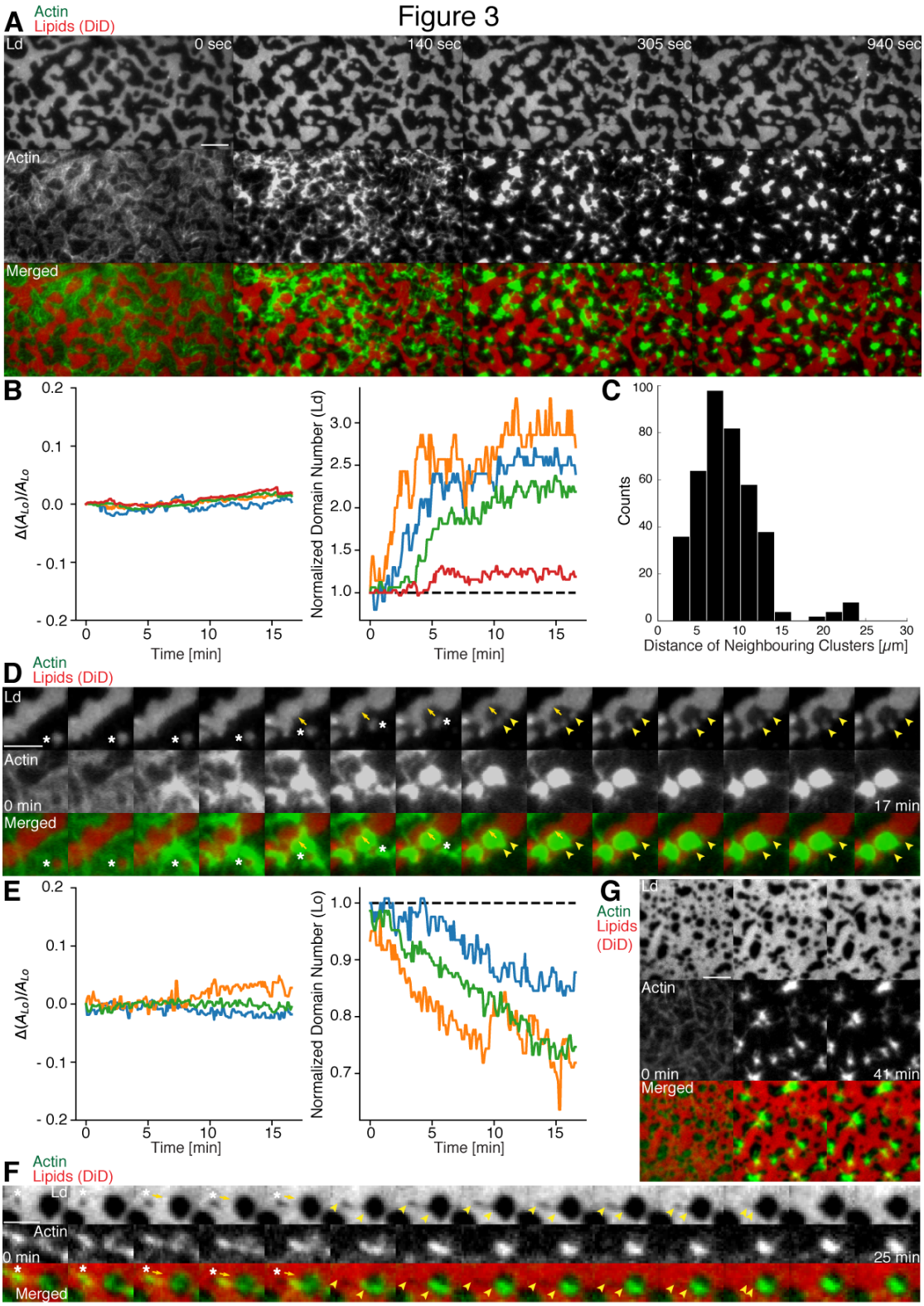

Fig. 3. Actomyosin contraction governs lateral membrane organization for various lipid compositions. (A) TIRFM time-lapse images of a contracting MAC with Alexa-488-phalloidin labeled actin filaments and DiD labeled L_d domains of a 1:2:1 DOPC:DPPC:Cholesterol mixture. Scale bar, 10 µm. (B) For the 1:2:1 DOPC:DPPC:Cholesterol mixture the area of the L_o phase was found to remain constant while the number of L_d domains increased with time through splitting. (C) Distance to neighboring actomyosin clusters for the lipid composition of 1:2:1 DOPC:DPPC:Cholesterol. (D) Representative example (1:2:1 DOPC:DPPC:Cholesterol mixture) showing movement (white asterisks) and deformation (inward ingression, yellow arrows) of a phase boundary upon actomyosin contraction and its splitting into two separated domains (yellow arrowheads). Scale bar, 10 µm. (E) For a lipid

composition of 3:3:1 DOPC:PSM:Cholesterol, the area of the L_o phase remained again constant and the number of L_o domains decreased. (F) Pulling of a L_o domain (white asterisk) for a lipid composition of 3:3:1 DOPC:PSM:Cholesterol by actomyosin led to fusion (yellow arrowheads) and relaxation into a larger neighboring domain. Scale bar, 2.5 µm. (G) Time-lapse montage of the actomyosin contraction on a 3:3:1 DOPC:PSM:Cholesterol phase-separated membrane. Small L_o domains are moved and fused to produce larger domains. Scale bar, 5 µm.

Figure 4

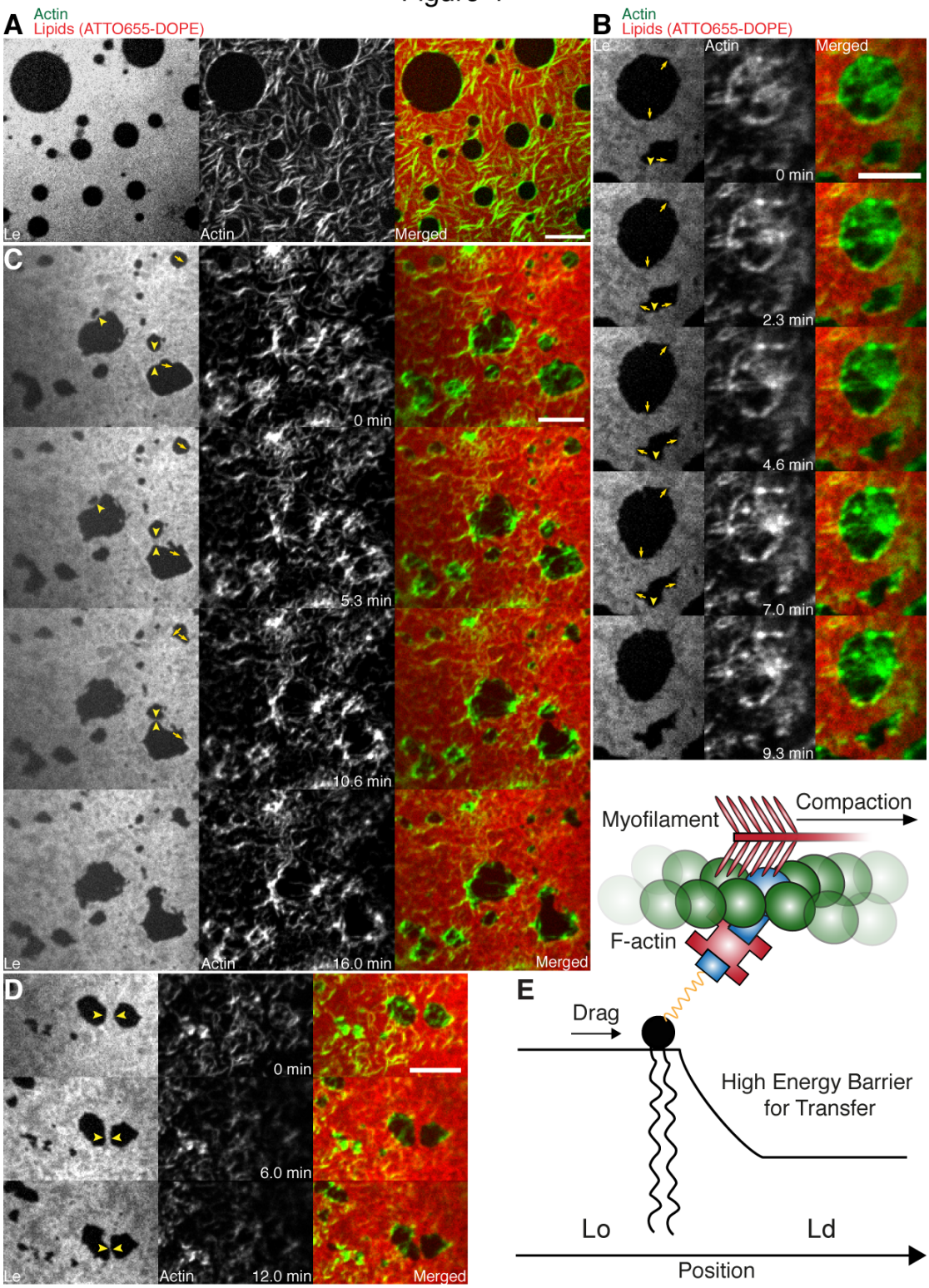

Fig. 4. Lipid monolayer domain shape changes and fusion events induced by actomyosin contractions. (A) Confocal Spinning Disk microscope images of Alexa-488-phalloidin labeled actin filaments coupled to a ATTO655-DOPE labeled lipid monolayer (3:3:1 DOPC:PSM:Cholesterol) in the absence

of myofilaments. Actin filaments close to the phase boundaries of lipid monolayer domains align to their circular shape. (B-D) Spinning Disk microscope time-lapse images of Alexa-488-phalloidin labeled actin filaments coupled to ATTO655-DOPE labeled lipid monolayers during myofilament induced contractions of actin filaments. Actomyosin contractions lead to shape changes and fusion events (yellow arrows and arrowheads) of the lipid monolayer L_c domains. (E) Scheme of a microscopic model. Scale bars, 10 µm.

Video legends

Video 1: Myosin induced actin rearrangements in a minimal actin cortex (MAC) combined with a supported phase-separated lipid bilayer

MAC with a supported phase-separated membrane (1:2:1 DOPC:DPPC:Cholesterol) containing Alexa-488-phalloidin labeled actin filaments (green) exhibits dynamic rearrangements of actin filaments after the addition of myofilaments in the presence of ATP and eventually forms actomyosin clusters. The phase-separated membrane containing DiD labeled L_d domains (red) is shown in the upper channel. The middle channel shows Alexa-488-phalloidin labeled actin filaments (green) that bind to the L_o domains. The lower channel shows the merge of both channels. TIRFM image sequence was acquired at 5 sec. time intervals and contains 200 frames. The video is displayed at 15 frames per second (fps). Total time: 16.6 min. Scale bar, 10 µm. (Compressed JPG avi; 10.2 MB).

Video 2: Shape changes, rearrangements and fusion events of L_d domains during actomyosin contraction

The phase-separated membrane (1:2:1 DOPC:DPPC:Cholesterol) containing DiD labeled L_d domains (red) is shown in the left channel. The middle channel shows Alexa-488-phalloidin labeled actin filaments that bind to the L_o domains. The right channel shows the merge of both channels. TIRFM image sequence was acquired at 5 sec. time intervals and contains 124 frames. The video is displayed at 15 frames per second (fps). Total time: 10.3 min. Scale bar, 10 µm. (Compressed JPG avi; 0.8 MB).

Video 3: Splitting, shape changes and deformations of L_d domains during actomyosin contraction

The phase-separated membrane (1:2:1 DOPC:DPPC:Cholesterol) containing DiD labeled L_d domains (red) is shown in the left channel. The middle channel shows Alexa-488-phalloidin labeled actin filaments that bind to the L_o domains. The right

356 channel shows the merge of both channels. TIRFM image sequence was acquired at 5
357 sec. time intervals and contains 200 frames. The video is displayed at 15 frames per
358 second (fps). Total time: 16.6 min. Scale bar, 10 µm. (Compressed JPG avi; 0.8 MB).
359
360 ***Video 4: L_d domain movement, splitting and ingression during actomyosin***
361 ***contraction***
362 The phase-separated membrane (1:2:1 DOPC:DPPC:Cholesterol) containing DiD
363 labeled L_d domains (red) is shown in the left channel. The middle channel shows
364 Alexa-488-phalloidin labeled actin filaments that bind to the L_o domains. The right
365 channel shows the merge of both channels. TIRFM image sequence was acquired at 5
366 sec. time intervals and contains 200 frames. The video is displayed at 15 frames per
367 second (fps). Total time: 16.6 min. Scale bar, 5 µm. Corresponds to Figure 3D.
368 (Compressed JPG avi; 0.4 MB).
369
370 ***Video 5: Shape changes, rearrangements and fusion events of L_o domains during***
371 ***actomyosin contraction***
372 The phase-separated and DiD labeled (red) membrane (3:3:1
373 DOPC:PSM:Cholesterol) containing L_o domains (dark) is shown in the upper channel.
374 The middle channel shows Alexa-488-phalloidin labeled actin filaments (green) that
375 bind to the L_o domains. The lower channel shows the merge of both channels. TIRFM
376 image sequence was acquired at 5 sec. time intervals and contains 500 frames. The
377 video is displayed at 15 frames per second (fps). Total time: 41.6 min. Scale bar, 10
378 µm. (Compressed JPG avi; 28 MB).
379
380 ***Video 6: Fusion event of a L_o domain during actomyosin contraction***
381 A small L_o domain is stretched by actin filaments thereby pulling the domain towards
382 a larger domain leading eventually to fusion of both L_o domains. The phase-separated
383 and DiD labeled (red) membrane (3:3:1 DOPC:PSM:Cholesterol) containing L_o
384 domains (dark) is shown in the left channel. The middle channel shows Alexa-488-
385 phalloidin labeled actin filaments (green) that bind to the L_o domains. The right
386 channel shows the merge of both channels. TIRFM image sequence was acquired at 5
387 sec. time intervals and contains 337 frames. The video is displayed at 120 frames per
388 second (fps). Total time: 28 min. Scale bar, 2.5 µm. Corresponds to Figure 3F.
389 (Compressed JPG avi; 0.4 MB).

390 ***Video 7: Disappearance of small L_o domains during actomyosin contraction***
391 Small L_o domains often vanish during actomyosin contractions. The phase-separated
392 and DiD labeled (red) membrane (3:3:1 DOPC:PSM:Cholesterol) containing L_o
393 domains (dark) is shown in the left channel. The middle channel shows Alexa-488-
394 phalloidin labeled actin filaments (green) that bind to the L_o domains. The right
395 channel shows the merge of both channels. TIRFM image sequence was acquired at 5
396 sec. time intervals and contains 493 frames. The video is displayed at 120 frames per
397 second (fps). Total time: 41 min. Scale bar, 5 µm. Corresponds to Figure 3G.
398 (Compressed JPG avi; 4.1 MB).
399
400 ***Video 8: Shape changes and fusion events during actomyosin contraction of L_c***
401 ***domains in a MAC combined with a phase-separated lipid monolayer***
402 Myofilaments in the presence of ATP led to the contraction of the actin layers and to
403 shape changes and fusion events of the L_c domains. The phase-separated lipid
404 monolayer (3:3:1 DOPC:PSM:Cholesterol) containing the ATTO655-DOPE labeled
405 L_e phase (red) is shown in the left channel. The middle channel shows Alexa-488-
406 phalloidin labeled actin filaments that bind to the L_e phase. The right channel shows
407 the merge of both channels. Confocal Spinning Disk image sequence was acquired at
408 20 sec. time intervals and contains 64 frames. The video is displayed at 15 frames per
409 second (fps). Total time: 21 min. Scale bar, 10 µm. Corresponds to Figure 4C.
410 (Compressed JPG avi; 1.7 MB).
411
412
413 ## Material and Methods
414
415 **Actin labeling and polymerization**
416 F-actin preparation was performed as described in (Vogel et al, 2013b). Briefly, a
417 39.6 µM actin solution (Actin/Actin-Biotin ratio of 5:1) was prepared by mixing
418 rabbit skeletal actin monomers (32 µl, 2 mg/ml, Molecular Probes) with biotinylated
419 rabbit actin monomers (1.6 µl, 10 mg/ml, tebu-bio/Cytoskeleton Inc.). F-buffer
420 (1 mM DTT, 1 mM ATP, 10 mM Tris-HCl (pH 7.4), 2 mM $MgCl_2$ and 50 mM KCl)
421 was added to the mixture in order to start polymerization. Actin polymers were
422 labeled and stabilized with Alexa Fluor 488 Phalloidin according to the

423 manufacturer's protocol (Molecular Probes). Finally, the 2 µM Alexa-488-Phalloidin
424 labeled biotinylated actin filament solution was stored at 4 °C.
425
426 **MAC (minimal actin cortex) preparation**
427 1,2-dioleoyl-*sn*-glycero-3-phosphorcholine (DOPC), 1,2-dipalmitoyl-*sn*-glycero-3-
428 phosphocholine (DPPC), and cholesterol were added in a molar ratio of 1:2:1 or
429 DOPC, N-palmitoyl-D-sphingomyelin (PSM), and Cholesterol in a molar ratio of
430 3:3:1 to a final lipid concentration of 5 mg/ml (Avanti Polar Lipids, Inc). The lipid
431 bilayer was further supplemented with 0.03 mol% DiD (Molecular Probes, Eugene,
432 OR) and 0.01, 0.1 or 1 mol% DSPE-PEG(2000)-Biotin (Avanti Polar Lipids, Inc.).
433 The solution was dried under continuous nitrogen flux and then placed under vacuum
434 for 1 h to remove chloroform residuals. The pellet was rehydrated in SLB buffer (150
435 mM KCl, 25 mM Tris-HCl, pH 7.5) by vigorous vortexing and sonication.

436 20 µl of clear lipid suspension was then diluted in 130 µl A-buffer (50 mM KCl, 2
437 mM $MgCl_2$, 1 mM DTT and 10 mM Tris-HCl, pH 7.5) and heated to 55°C.
438 Meanwhile, freshly cleaved mica was fixated with immersion oil (Carl Zeiss, Jena,
439 Germany) on a cover slip (22x22 mm, #1.5, Menzel Gläser, Thermo Fisher) and
440 covered with the center part of a cut 1.5 mL Eppendorf tube. The Eppendorf tube was
441 glued with UV-sensitive glue (Norland Optical Adhesive 63, Cranbury, USA). The
442 chamber was filled with 75 µl of small unilamellar vesicles and incubated at 55 °C for
443 45 minutes with 1 mM $CaCl_2$. Non-fused vesicles were removed by washing the
444 suspension with 2 ml warmed A-buffer and gentle pipetting. The chamber's
445 temperature was slowly cooled. Next, 2 µl of unlabeled or Oregon-Green labeled
446 neutravidin (1mg/ml, Molecular Probes) diluted in 200 µl A-buffer were added to the
447 sample and incubated for 10 min. Finally, unbound proteins were removed by gently
448 washing the solution with 2 ml A-buffer.

449 **Phase separation with MAC**
450 The phase-separated membrane was heated with an objective heater (Carl Zeiss, Jena,
451 Germany) to the setpoint of 42 °C and cooled down to 30 °C, both with and without
452 Alexa-488-Phalloidin labeled biotinylated actin filaments. The area distribution of
453 domains at equilibrium (45 min after 30 °C was reached) was then compared between
454 the different concentrations of DSPE-PEG(2000)-Biotin (0.1, 0.01 mol%).

455 **Crowding-Effect**

456 The sample was placed on the TIRF microscope objective with attached objective
457 heater and slowly warmed to the setpoint of 42 °C. The lipid bilayer with 1.0 %
458 DSPE-PEG(2000)-Biotin was equilibrated at different temperatures below the melting
459 point (~37 °C for 1:2:1 DOPC:DPPC:Cholesterol). 20 µl of Alexa-488-Phalloidin
460 labeled biotinylated actin filaments were then carefully added to the chamber. Binding
461 of actin filaments to the membrane was recorded by acquiring images in interleaved
462 mode (488 nm and 640 nm) every 2.5 seconds, generating a time-lapse movie with a 5
463 sec delay between subsequent images.

464

465 **F-actin network contraction by myofilaments**

466 After the addition of 20 µl Alexa-488-Phallodin labeled biotinylated actin filaments to
467 the supported lipid bilayer at room temperature (~24 °C), the mixture was incubated
468 for approximately 45 min in order to ensure full binding of actin filaments to the
469 membrane. Subsequently, residual actin was removed by gently exchanging the
470 solution with 2 ml A-buffer. Once the properly assembled MAC was verified with
471 TIRF microscopy, a solution of 20 µl myofilaments and 1 µl ATP (0.1 M) were added
472 to start the compaction of actin filaments.

473 Images were acquired every 2.5 sec in interleaved mode, which eliminated the cross
474 talk between color channels of actin filaments and the phase-separated membrane.

475

476 **TIRF microscopy**

477 Fluorescent imaging of labeled proteins and membrane was carried out on a custom-
478 built TIRF microscope. The setup was integrated into an Axiovert 200 microscope
479 (Zeiss). The probe was illuminated and imaged through a Plan-Apochromat 100x/NA
480 1.46 oil immersion objective with a 488-nm and 630-nm laser. Images were acquired
481 with an Andor Solis EMCCD camera (electron gain = 300, exposure time = 50 ms,
482 frame interval = 2.5 or 5 sec) in interleaved mode.

483

484 **Data analysis**

485 Image processing, analysis and data visualization was performed with Fiji and the
486 scientific packages for Python. Multichannel beads were used to align double-color
487 image stacks with the Fiji plugin Descriptor-based series registration. The contour

488 length between the lipid domains was extracted by detecting edges (Canny edge
489 detection; (van der Walt et al, 2014)) in single fluorescent images acquired from
490 phase-separated membranes. The contour length over time was fitted to $L =$
491 $L_{Final}\,(1 - \exp(-1/\tau\,(t - t_0)))$ with $t_0 = 1$ min. The actomyosin clusters were
492 detected using the Laplacian of Gaussian method (scikit-image (van der Walt et al,
493 2014)) and assigned to neighbors using the Delaunay triangulation and its method
494 vertex_neighbor_vertices.
495 To detect the lipid domains, the fluorescence images were firstly corrected for an
496 uneven background signal. Then, the DiD signal was classified with a local adaptive
497 thresholding algorithm and the corresponding phase boundaries with the Canny edge
498 detection algorithm. The binary image stacks were combined with the XOR operator
499 and further refined using the morphological closing operation. Small holes were
500 removed from the binary images. Small objects were detected with the Laplacian of
501 Gaussian method and as a final step, combined with the binary images. The script was
502 implemented in Python with the image processing package scikit-image.
503

504 **MAC assembly on lipid monolayers**

505 For the lipid monolayer assays the same lipid mixtures and molar ratios were used as
506 for the supported bilayers with 1 mol% of DSPE-PEG(2000)-Biotin. The lipids were
507 mixed, dried under nitrogen flux for 15 min, subsequently put into vacuum for 30 min
508 and dissolved in chloroform (total lipid concentration of 1 mg/ml). The mixtures were
509 further diluted to a final lipid concentration of 0.1 mg/ml and labeled by addition of
510 0.1 mol% of ATTO655-DOPE (ATTO-TEC GmbH, Siegen, Germany). The total
511 lipid concentration was confirmed by gravimetry.

512 To form a chamber (see Scheme 1), chamber spacers were cut from a 5mm thick sheet
513 of PTFE by a laser cutter. The spacers were sonicated step by step in acetone,
514 chloroform, isopropanol and ethanol (15 min each). Glass cover slips of 15 mm
515 (Gerhard Menzel GmbH, Braunschweig, Germany) were fixed to the spacer by
516 picodent twinsil® 22 two component glue (picodent®, Wipperfuerth, Germany). The
517 chambers were washed alternately with ethanol and water, air dried and air plasma-
518 cleaned for 10 min in order to make the glass hydrophilic. The surface was then
519 passivated by covering the glass surface with PLL-PEG(2000) (SuSos AG,

520 Dübendorf, Switzerland) 0.5 mg/mL solution in PBS buffer and incubated for
521 minimum half an hour. After throughout wash with water (5 times 200 µl) and
522 reaction buffer (3 times 200 µl), the chambers were ready to use.
523 Lipid monolayers were formed by drop-wise deposition of the lipid mixture on the
524 buffer-air interface (for further details, see also (Chwastek & Schwille, 2013)). A lipid
525 mixture volume corresponding to a lipid surface density of 70 $Å^2$ / molecule was
526 deposited drop-wise on the surface of the buffer solution.

527 The samples were imaged using a Yokogawa scan head CSU10-X1 spinning disk
528 system connected to a Nikon Eclipse Ti inverted microscope (Nikon, Japan) with an
529 Andor Ixon Ultra 512x512 EMCCD camera and a 3i solid state diode laser stack with
530 488 nm, 561 nm and 640 nm laser lines (3il33, Denver, Colorado USA). For
531 simultaneous Alexa-488-phalloidin and ATTO655-DOPE excitation, the 488 nm and
532 the 640 nm laser lines and an UPLanSApo 60x/1.20 Water UIS2 objective (Olympus,
533 Japan) were used. The time interval between the recorded images was 20 s.

534 After confirming the formation of a phase-separated lipid monolayer by imaging,
535 100 µl of neutravidin solution (0.01 µg/µl) was added to the sample twice and was
536 incubated for 5 min. Note that all protein solutions or other solutions are applied
537 directly to the liquid subphase by dipping the pipette tip through the monolayer. Next,
538 the subphase was washed 5 times with buffer (100 µl steps) to remove unbound
539 neutravidin. Subsequently, 20 µl of Alexa-488-phalloidin labeled actin filaments
540 (2 µM) was added to the subphase and incubated for at least 60 min, since binding of
541 actin filaments to the interface was assumed to occur relatively slowly. When the
542 binding of the actin filaments was confirmed by imaging, the monolayer was
543 thoroughly washed (7 to 10 steps of 100 µl) with reaction buffer containing 1 µM
544 ATP and 100 µl of myofilaments (0.3 µM) containing 1 µM ATP (enzymatically
545 regenerated see above) was added to the subphase twice. The sample was sealed by a
546 glass cover slide with grease to avoid subphase evaporation, allowing for long sample
547 observation. The lipid monolayer MAC system started to contract after a few minutes
548 of incubation, resulting in the formation of actomyosin clusters and deformation of
549 the lipid domains.

550

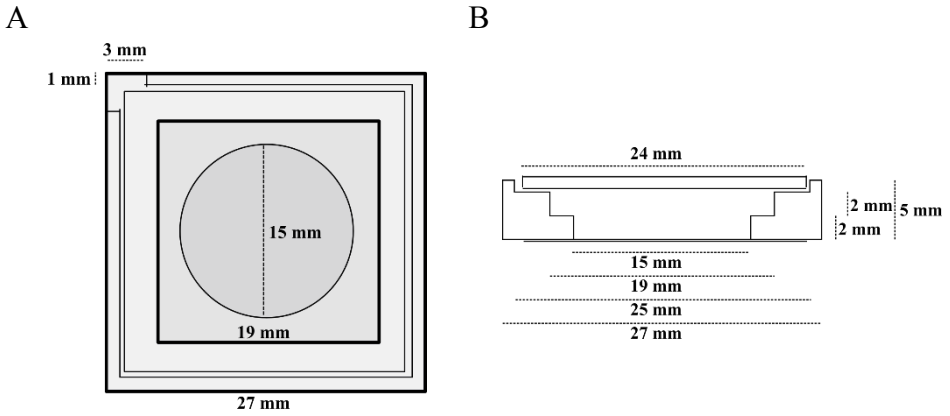

Scheme 1: Top (A) and lateral (B) schematic view of the PTFE chamber (adapted from (Chwastek & Schwille, 2013).

Acknowledgements

We are grateful for the financial support by the Daimler und Benz foundation (Project Grant PSBioc8216), the Gottfried Wilhelm Leibniz-Program of the DFG **(**SCHW716/8-1**),** the support of the Graduate School of Quantitative Biosciences Munich and the MaxSynBio consortium, which is jointly funded by the Federal Ministry of Education and Research of Germany and the Max Planck Society.

References

Akimov SA, Kuzmin PI, Zimmerberg J, Cohen FS (2007) Lateral tension increases the line tension between two domains in a lipid bilayer membrane. *Phys Rev E* **75**

Arumugam S, Petrov EP, Schwille P (2015) Cytoskeletal pinning controls phase separation in multicomponent lipid membranes. *Biophys J* **108:** 1104-1113

Backouche F, Haviv L, Groswasser D, Bernheim-Groswasser A (2006) Active gels: dynamics of patterning and self-organization. *Phys Biol* **3:** 264-273

Baumgart T, Hess ST, Webb WW (2003) Imaging coexisting fluid domains in biomembrane models coupling curvature and line tension. *Nature* **425:** 821-824

Chwastek G, Schwille P (2013) A monolayer assay tailored to investigate lipid-protein systems. *Chemphyschem* **14:** 1877-1881

583 Engelman DM (2005) Membranes are more mosaic than fluid. *Nature* **438:** 578-580
584
585 Garcia-Saez AJ, Chiantia S, Schwille P (2007) Effect of line tension on the lateral
586 organization of lipid membranes. *The Journal of biological chemistry* **282:** 33537-
587 33544
588
589 Gowrishankar K, Ghosh S, Saha S, C R, Mayor S, Rao M (2012) Active remodeling
590 of cortical actin regulates spatiotemporal organization of cell surface molecules. *Cell*
591 **149:** 1353-1367
592
593 Groves JT, Kuriyan J (2010) Molecular mechanisms in signal transduction at the
594 membrane. *Nat Struct Mol Biol* **17:** 659-665
595
596 Gudheti MV, Curthoys NM, Gould TJ, Kim D, Gunewardene MS, Gabor KA, Gosse
597 JA, Kim CH, Zimmerberg J, Hess ST (2013) Actin mediates the nanoscale membrane
598 organization of the clustered membrane protein influenza hemagglutinin. *Biophys J*
599 **104:** 2182-2192
600
601 Heinemann F, Vogel SK, Schwille P (2013) Lateral membrane diffusion modulated
602 by a minimal actin cortex. *Biophys J* **104:** 1465-1475
603
604 Honerkamp-Smith AR, Cicuta P, Collins MD, Veatch SL, den Nijs M, Schick M,
605 Keller SL (2008) Line tensions, correlation lengths, and critical exponents in lipid
606 membranes near critical points. *Biophys J* **95:** 236-246
607
608 Honigmann A, Sadeghi S, Keller J, Hell SW, Eggeling C, Vink R (2014) A lipid
609 bound actin meshwork organizes liquid phase separation in model membranes. *Elife*
610 **3:** e01671
611
612 Koster DV, Husain K, Iljazi E, Bhat A, Bieling P, Mullins RD, Rao M, Mayor S
613 (2016) Actomyosin dynamics drive local membrane component organization in an in
614 vitro active composite layer. *Proc Natl Acad Sci U S A*
615
616 Kuzmin PI, Akimov SA, Chizmadzhev YA, Zimmerberg J, Cohen FS (2005) Line
617 tension and interaction energies of membrane rafts calculated from lipid splay and tilt.
618 *Biophysical Journal* **88:** 1120-1133
619
620 Liu AP, Fletcher DA (2006) Actin polymerization serves as a membrane domain
621 switch in model lipid bilayers. *Biophys J* **91:** 4064-4070
622
623 Luo W, Yu CH, Lieu ZZ, Allard J, Mogilner A, Sheetz MP, Bershadsky AD (2013)
624 Analysis of the local organization and dynamics of cellular actin networks. *J Cell Biol*
625 **202:** 1057-1073
626
627 Munro E, Nance J, Priess JR (2004) Cortical flows powered by asymmetrical
628 contraction transport PAR proteins to establish and maintain anterior-posterior
629 polarity in the early C. elegans embryo. *Developmental cell* **7:** 413-424
630
631 Murase K, Fujiwara T, Umemura Y, Suzuki K, Iino R, Yamashita H, Saito M,
632 Murakoshi H, Ritchie K, Kusumi A (2004) Ultrafine membrane compartments for

633 molecular diffusion as revealed by single molecule techniques. *Biophysical journal*
634 **86:** 4075-4093
635
636 Murrell MP, Gardel ML (2012) F-actin buckling coordinates contractility and
637 severing in a biomimetic actomyosin cortex. *Proc Natl Acad Sci U S A* **109:** 20820-
638 20825
639
640 Sheetz MP, Schindler M, Koppel DE (1980) Lateral mobility of integral membrane
641 proteins is increased in spherocytic erythrocytes.
642
643 Simons K, Gerl MJ (2010) Revitalizing membrane rafts: new tools and insights.
644 *Nature Reviews Molecular Cell Biology* **11:** 688-699
645
646 Soares e Silva M, Depken M, Stuhrmann B, Korsten M, MacKintosh FC, Koenderink
647 GH (2011) Active multistage coarsening of actin networks driven by myosin motors.
648 *Proc Natl Acad Sci U S A* **108:** 9408-9413
649
650 van der Walt S, Schonberger JL, Nunez-Iglesias J, Boulogne F, Warner JD, Yager N,
651 Gouillart E, Yu T, scikit-image c (2014) scikit-image: image processing in Python.
652 *PeerJ* **2:** e453
653
654 Veatch SL, Cicuta P, Sengupta P, Honerkamp-Smith A, Holowka D, Baird B (2008)
655 Critical fluctuations in plasma membrane vesicles. *Acs Chem Biol* **3:** 287-293
656
657 Veatch SL, Keller SL (2003) Separation of liquid phases in giant vesicles of ternary
658 mixtures of phospholipids and cholesterol. *Biophys J* **85:** 3074-3083
659
660 Veatch SL, Keller SL (2005) Miscibility phase diagrams of giant vesicles containing
661 sphingomyelin. *Phys Rev Lett* **94:** 148101
662
663 Veatch SL, Polozov IV, Gawrisch K, Keller SL (2004) Liquid domains in vesicles
664 investigated by NMR and fluorescence microscopy. *Biophys J* **86:** 2910-2922
665
666 Verkhovsky AB, Svitkina TM, Borisy GG (1997) Polarity sorting of actin filaments
667 in cytochalasin-treated fibroblasts. *Journal of cell science* **110 (Pt 15):** 1693-1704
668
669 Vogel SK (2016) Reconstitution of a Minimal Actin Cortex by Coupling Actin
670 Filaments to Reconstituted Membranes. *Methods Mol Biol* **1365:** 213-223
671
672 Vogel SK, Heinemann F, Chwastek G, Schwille P (2013a) The design of MACs
673 (minimal actin cortices). *Cytoskeleton (Hoboken)* **70:** 706-717
674
675 Vogel SK, Petrasek Z, Heinemann F, Schwille P (2013b) Myosin Motors Fragment
676 and Compact Membrane-Bound Actin Filaments. *eLife* **2013;2:e00116**
677
678 Yang ST, Kiessling V, Tamm LK (2016) Line tension at lipid phase boundaries as
679 driving force for HIV fusion peptide-mediated fusion. *Nature communications* **7**
680
681
682